Numerical study of the delamination toughening effect of weakening and toughening patche

Trabal, Guillem Gall; Bak, Brian Lau Verndal; Chen, B. Y.; Jensen, Simon Mosbjerg; Lindgaard, Esben

Important note
To cite this publication, please use the final published version (if applicable).
Please check the document version above.

ECCM 20

26–30 JUNE 2022
LAUSANNE SWITZERLAND
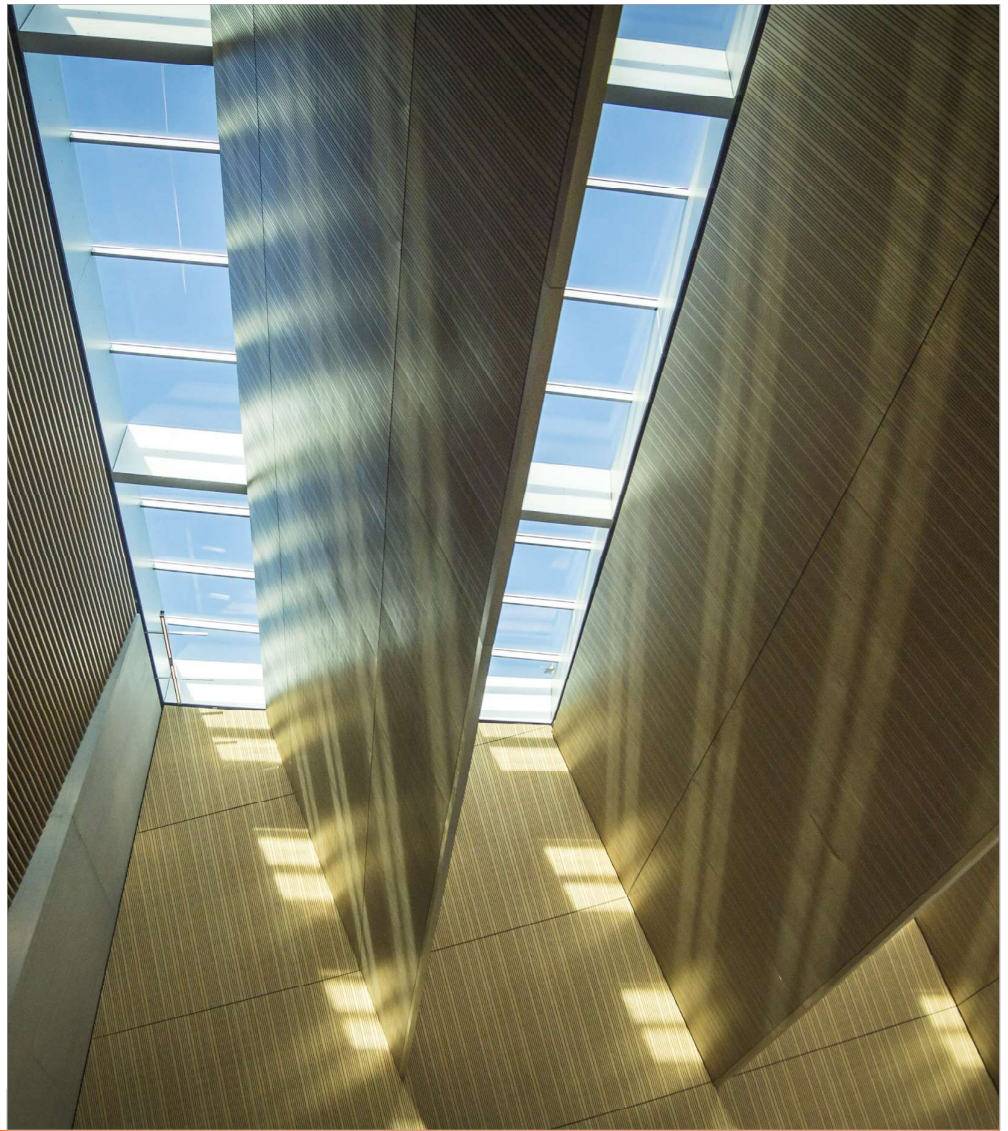
Proceedings
of the 20th European Conference
on Composite Materials

COMPOSITES MEET SUSTAINABILITY

Vol 4 – Modeling and Prediction

Editors : Anastasios P. Vassilopoulos, Véronique Michaud

Proceedings of the 20th
European Conference on Composite Materials
ECCM20
26-30 June 2022,
EPFL Lausanne Switzerland

Edited By :

Prof. Anastasios P. Vassilopoulos, CCLab/EPFL
Prof. Véronique Michaud, LPAC/EPFL

Oragnized by:

Composite Construction Laboratory (CCLab)
Laboratory for Processing of Advanced Composites (LPAC)
Ecole Polytechnique Fédérale de Lausanne (EPFL)

Published by :

Cover:

Swiss Tech Convention Center
© Edouard Venceslau - CompuWeb SA

Cover Design:

Composite Construction Laboratory (CCLab)
Ecole Polytechnique Fédérale de Lausanne (EPFL)
Lausanne, Switzerland

©2022 ECCM20/The publishers

Disclaimer:

The ECCM20 organizing committee and the Editors of these proceedings assume no responsibility or liability for the content, statements and opinions expressed by the authors in their corresponding publication.

NUMERICAL STUDY OF THE DELAMINATION TOUGHENING EFFECT OF WEAKENING AND TOUGHENING PATCHES

Guillem Gall Trabal[a], Brian Lau Verndal Bak[a], Boyang Chen[b], Simon Mosbjerg Jensen[a],Esben Lindgaard*[a]

a: CraCS research group (cracs.aau.dk), Department of Materials and Production, Aalborg University, Fibigerstræde 16, Aalborg, Denmark *(elo@mp.aau.dk)
b: Faculty of Aerospace Engineering, Delft University of Technology, Kluyverweg 1, 2629HS Delft, Netherlands

Abstract: *A numerical study on the feasibility of using patches of interface weakening or toughening material to trigger multiple delaminations toughening laminated composite structures against delamination is presented. The studies use an adaptive refinement formulation that uses cohesive elements to model delamination initiation and propagation. A DCB specimen is loaded under displacement control with two cohesive interfaces and a single pre-crack is introduced in one of them. The studies show that multiple delaminations can be initiated in the secondary originally uncracked interface by placing interface toughening patches at the main pre-cracked interface or interface weakening patches at the secondary one. The energy dissipation significantly increases compared to a standard DCB specimen featuring a single delamination.*

Keywords: Delamination toughening; multiple delamination, adaptive refinement, cohesive zone modelling; Floating Node Method

1. Introduction

Several methodologies have been introduced in the literature to toughen composite laminated structures against delamination propagation. Current strategies include modifying the constituent materials by improving the interface between fibre and matrix using fibre sizing [1,2] or obtaining tougher matrix materials. Interface toughening can also be obtained by procedures such as stitching [3,4], z-pinning [5], interlocking mechanisms [6], or using 3D woven fabrics [7]. However, the aforementioned techniques provoke unwanted side effects such as a decrease in the wettability of the laminate or a decrease in the in-plane strength of the structure [5].

Another option is to toughen the structure by defusing the damage into multiple delamination fronts. This idea, presented in [8], implemented using a weakened interface, increases the amount of energy dissipated. However, creating a weakened plane may induce premature damage initiation from e.g., intralaminar damage. Another option noticed for toughened interfaces in co-cured laminates [9] is using a local toughening of the interface to initiate damage in a secondary adhesive interface.

In this article, the possibility of onsetting multiple delaminations in laminated composites using patches of interface toughening or weakening material is explored with a set of numerical tests featuring different interface toughening or weakening materials. The analyses are performed with a modified version of the adaptive refinement formulation from [10].

2. Methods and numerical testing protocol

This section introduces the methodology and numerical testing protocol used to study the interface patching induced multiple delamination initiation, and the toughening effect it has on the structure.

2.1 Adaptive refinement formulation

The adaptive Floating Node Method (FNM) based formulation presented in [10] is composed of the Adaptive Refinement Scheme (ARS) and the Adaptive FNM (A-FNM) element. Together, the ARS and the A-FNM element efficiently refine the model as required, obtaining a computationally efficient formulation for the accurate analysis of delamination propagation using Cohesive Zone Models (CZM). The adaptive formulation presented in [10] does not consider damage initiation in pristine interfaces, a feature needed for the numerical tests presented in this work. All the modifications to the adaptive formulation necessary for the work presented in this paper are restricted to the ARS. Therefore, the A-FNM element is not presented in this section, and the reader is instead referred to [10] for details.

The formulation presented in [10] allows the discretisation of an entire 2D laminate with a single A-FNM element through the thickness, as shown in Figure 1a. Each of the A-FNM elements contains a set of interfaces that can be at 4 different states: 1) Fully damaged, 2) Refined, 3) Coarse, or 4) Pristine. For the cases analysed in this paper, only states 1), 2) and 3) are relevant.
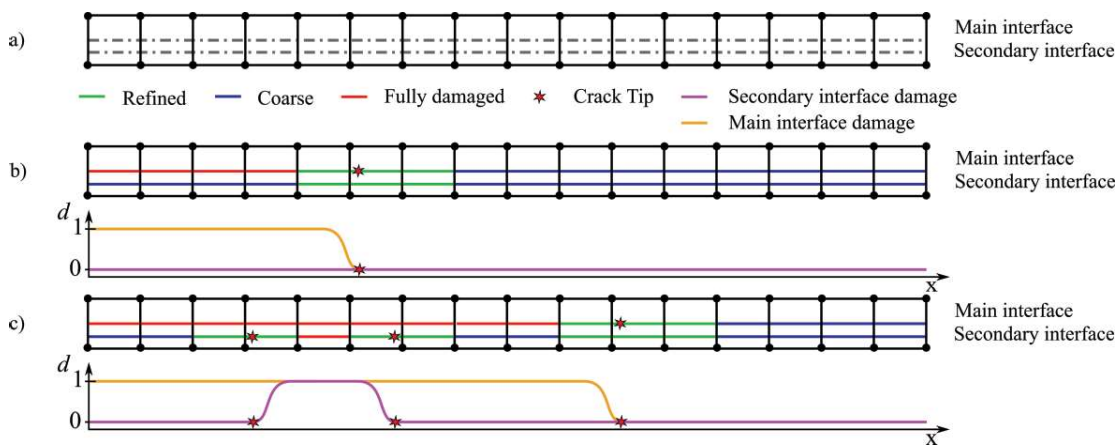
Figure 1: Adaptive Floating Node Method (A-FNM) element interface states of the specimen shown in a), after the application of the ARS for a single delamination b), and after the initiation of multiple delaminations c).

The ARS algorithm continuously monitors the damage in the structure to allocate the correct state at each A-FNM element interface in the model. As visualised in Figure 1b, the ARS sets all the A-FNM elements containing damage and its immediate neighbours to a refined state. The A-FNM element interfaces that have been fully damaged are set at a damaged state, and the remaining A-FNM element interfaces are set as coarse. With this approach, the damaged interfaces and their surroundings are effectively refined, leaving the remaining ones with a coarse discretisation of damaged or undamaged cohesive elements.

The fact that all the undamaged A-FNM element interfaces of the model contain at least a coarse cohesive element allows damage initiation in pristine interfaces. This is exemplified by the

scenario shown in Figure 1, which is encountered in the studies presented in this article. Initially, a single delamination propagates through the structure, as seen in Figure 1b. Notice how the secondary interface near the crack tip is at a refined state. This refinement allows for the accurate initiation of damage, which can eventually form two new independent crack tips, as seen in Figure 1c. Thus, the only necessary change to the ARS is allowing the preallocation of coarse CEs at any interface (pre-cracked or pristine) selected by the user.

2.2 Underlying standard element formulations

The calculation of the A-FNM element stiffness matrix is done by assembling stiffness matrices calculated for each of the sub-elements. The subelements are shown in Figure 2 for the relevant configurations of the presented numerical studies. The solid sub-elements stiffness matrices are calculated following a 4-node Enhanced Assumed Strains plane strain layered formulation detailed in [10]. This formulation enables the use of coarse discretisations under bending dominated situations and the use of a single sub-element to model several layers. The cohesive sub-elements are formulated as cohesive interface elements following the formulations presented in [11,12] adapted to a 4-node interface configuration.
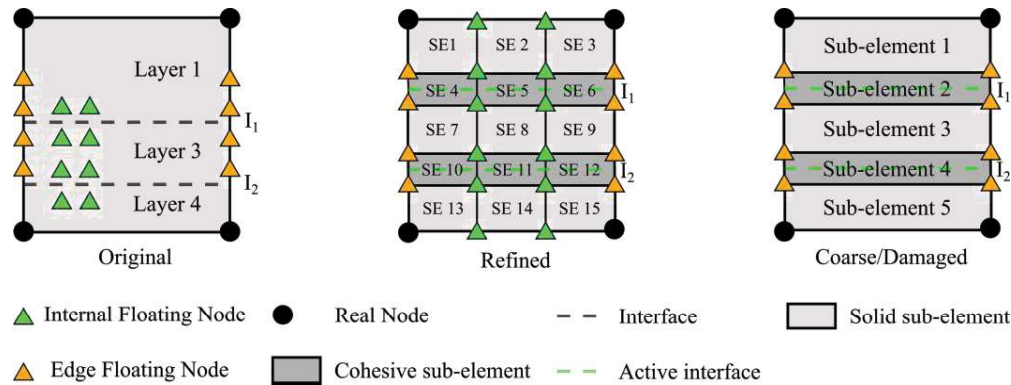
Figure 2: The A-FNM element's three configurations in the numerical tests.

2.3 Numerical testing protocol

A set of tests are performed with the specimen shown in Figure 3. The specimen contains either a toughening or a weakening interface material patch. The base material used for the analyses is listed in

Tabel 1. An initial mesh of 90 A-FNM elements is used, resulting in the initial mesh shown in Figure 4. A cohesive sub-element size of 0.084 mm is chosen in the refined area to ensure that a minimum of 4 cohesive sub-elements are present in the damage process zone.

Figure 3: Specimen used in the numerical tests. Dimensions in [mm]

Tabel 1: Base material and interface properties used in the numerical tests [13,14].

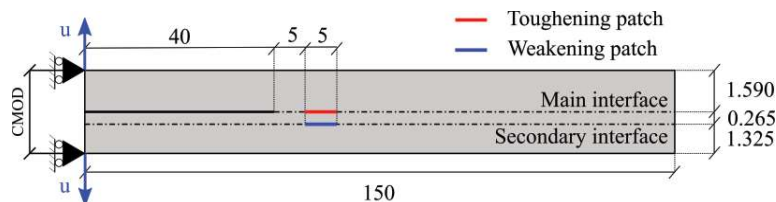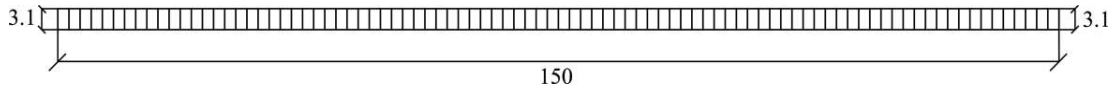| Material properties			Interface properties		
E_{11}	120	[GPa]	G_{Ic}	260	[N/m]
$E_{22} = E_{33}$	10.5	[GPa]	G_{IIc}	1002	[N/m]
$G_{12}=G_{13}$	5.3	[GPa]	τ_{I0}	30	[N/m]
G_{23}	3.5	[GPa]	τ_{II0}	60	[N/m]
$\nu_{12}= \nu_{13}$	0.3	[-]	η	2.73	[-]
ν_{23}	0.51	[-]	K	30e6	[N/mm^3]

Figure 4: Initial coarse mesh of A-FNM elements. Dimensions in mm.

A total of 50 numerical tests are performed. These are grouped in 2 categories featuring either an interface toughening patch or an interface weakening patch. The interface patches are modelled by changing the interface properties at the designated patched areas. This is done by multiplying or dividing the onset tractions (τ_{I0}, τ_{II0}) by an integer scalar *n,* and the critical energy release rates (G_{Ic}, G_{IIc}) by an integer scalar *m*:

$$(G_c \cdot n, \tau_0 \cdot m) \rightarrow \text{Interface toughening patch}$$
$$(G_c/n, \tau_0/m) \rightarrow \text{Interface weakening patch}$$

The 25 analyses for each category are built by varying *n* and *m* from 1 to 5 in unity steps.

3. Results

3.1 General response

The force-displacement equilibrium curve for the analyses featuring an interface toughening patch and those with an interface weakening patch are displayed in Figure 5 and Figure 6, respectively.

Figure 5: Force-displacement equilibrium curves for the analyses featuring an interface toughening patch.

Notice, that cases where multiple delaminations are initiated, display a response with higher force level than the single delamination reference case ($1 \cdot \tau_0, 1 \cdot G_c$) during the crack propagation phase. In that regard, both interface toughening and weakening patches can initiate multiple delaminations. Figure 5 also shows that the interface toughening patch approach results in a higher force peak than the interface weakening patch strategy results from Figure 6.
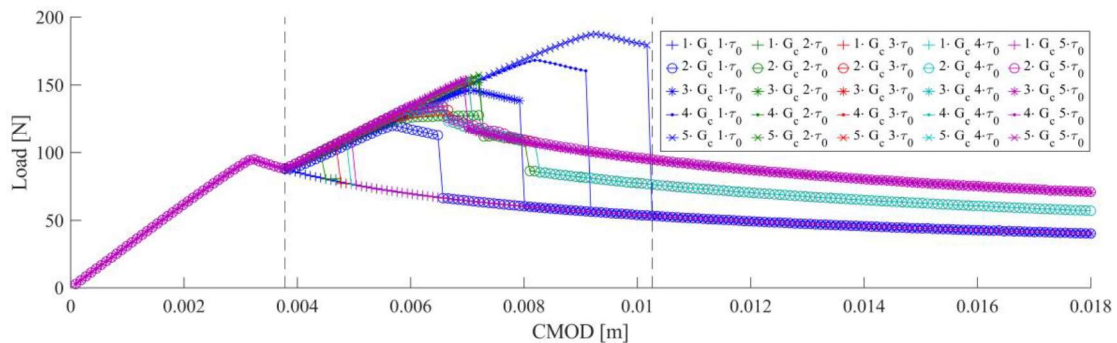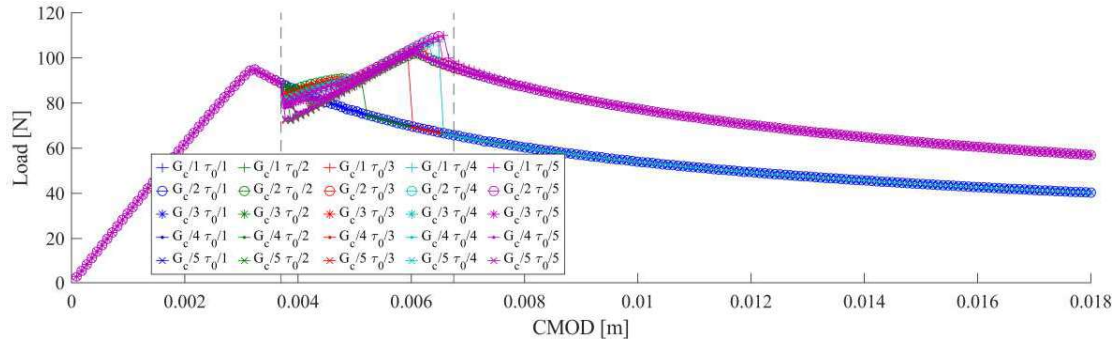
Figure 6: Force-displacement equilibrium curves for the analyses featuring an interface weakening patch.

3.2 Multiple delamination initiation

To study the delamination initiation phase, the normalised traction $\tilde{\mu}$, and the energy-based damage variable D_e [14] are defined as:

$$\tilde{\mu} = \frac{\mu}{\mu_0} \quad where \ \mu_0 = \sqrt{\tau_{I0}^2 + (\tau_{II0}^2 - \tau_{I0}^2)B^\eta}$$

$$D_e = \frac{G_c - \omega_r}{G_c} = 1 - \frac{\lambda_c(1 - D)K\lambda_D}{2G_c}$$

where ω_r is the specific remaining ability to do non-conservative work, and λ_D, λ_c are defined as in [14]. Figure 7 shows the multiple delaminations initiation process. When the traction profile enters the patched area, the increase in the traction peak produced by the interface toughening patch initiates the damage at the secondary interface. This happens because the secondary interface properties are unmodified, unlike in the main interface. The same case also holds for the interface weakening patch, but in this case, the main interface traction profile is not varied when entering the patched area. The decrease in the interface onset traction value produces the damage initiation. In both cases, the toughness of the interface at the patched area needs to be modified to extend the damage in an area sufficiently large to initiate the two new delamination fronts.
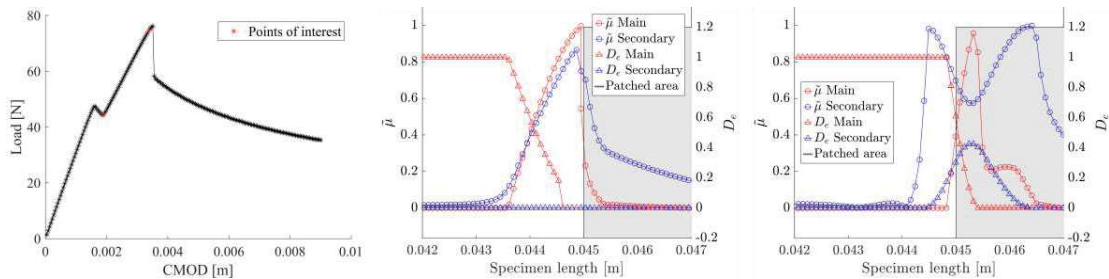
Figure 7: Normalized traction and damage D_e for a toughening patch of (G_c·3,τ_0·3) at selected points of interest.

3.3 Multiple delaminations propagation phase

The propagation phase of the analyses shown in Figure 5 andFigure 6 is determined by whether multiple delaminations are initiated and if so which crack tips are propagating. Figure 8 shows the energy dissipation rate defined as the energy dissipated per crack mouth opening (CMOD).

In both cases, the analyses with multiple delaminations initiation (curves 2 and 3) provide higher energy dissipation than the single delamination cases (curve 1).

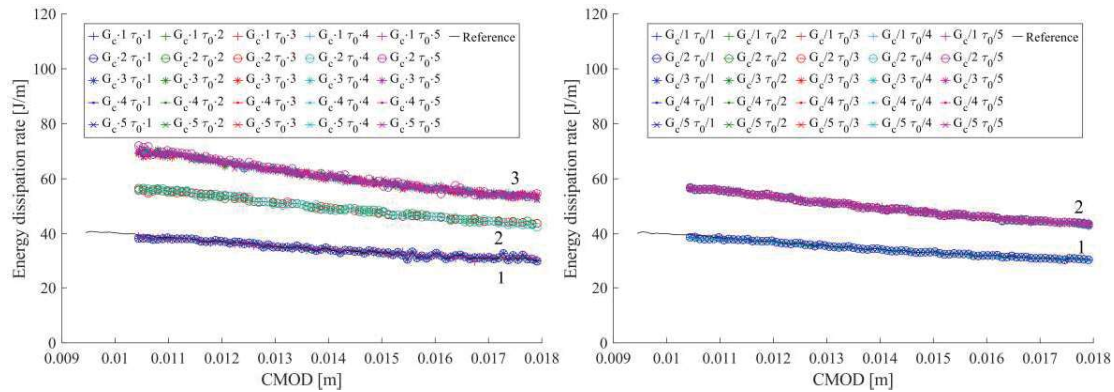Figure 8: Energy dissipation rate for the interface toughening (left) and weakening (right) analyses.

The three different curves displayed in Figure 8 are linked to the three outcomes displayed in Figure 9. Outcome 1 is the reference case with a single delamination, where multiple delaminations is not initiated. Outcome 2 occurs when multiple delaminations are onset in the interface weakening cases, and in the interface toughening cases where the main crack is not arrested. For interface toughening cases with a high G_{Ic} and G_{IIc}, outcome 3, the main crack tip is successfully arrested, leaving the crack tips at the secondary interface as the only ones propagating. This situation results in more energy dissipation due to the local mode mixity conditions, which have a higher mode II component.
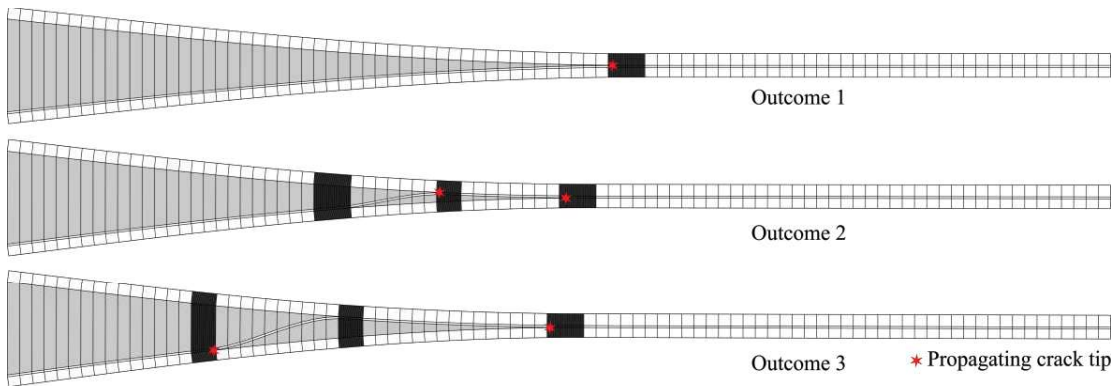

Figure 9: Deformed mesh at the end of selected analyses.

4. Discussion and Conclusions

A study on the toughening effect against delamination propagation produced by initiating multiple delaminations by including interface toughening or weakening patches in the structure is presented. A set of numerical tests is performed using a slightly modified version of the FNM adaptive formulation from [10]. The studies show that multiple delaminations can be initiated with both interface weakening and toughening patches, with overall higher load carrying capabilities provided by the analyses featuring a toughening patch. Moreover, the studied traction profiles identify that the multiple delaminations initiation is driven by a combination of onset traction and toughness modification of the patched area. Different outcomes depending on the values of the patched area onset traction and toughness are observed. The different

outcomes are a consequence of the multiple delaminations initiation, and of which crack tips propagate afterwards. Each of the outcomes corresponds to a different level of energy dissipation. The presented studies for quasi-static loading show promising results for increasing the toughness and load carrying ability. As a next step, the authors would like to explore how significant these effects will be for more advanced cohesive law formulations able to capture the effects of fibre bridging [15,16]. Furthermore, the authors would like to explore the effects of the interface weakening and toughening patches on fatigue-driven damage initiation and propagation. To accomplish this, the authors will use the fatigue simulation framework [17,18,19] which has recently been implemented into the A-FNM framework.

Acknowledgements

References

1. Wu Z, Yi XS, Wilikinson A. Interlaminar fracture toughness of carbon fibre/RTM6-2 composites toughened with thermoplastic-coated fabric reinforcement. Composites Part B: Engineering. 2017 December; 130: 192-199.

2. Downey MA, Drzal LT. Toughening of carbon fiber-reinforced epoxy polymer composites utilizing fiber surface treatment and sizing. Composites Part A: Applied Science and Manufacturing. 2016 November; 90: 687-698.

3. Göktaş D, Kennin WR, Potluri P. Improvement of Mode I Interlaminar Fracture Toughness of Stitched Glass/Epoxy Composites. Appl Compos Mater. 2017 April; 24: 351-375.

4. Ravandi M, Teo WS, Tran LQN, Yong MS, Tay TE. The effects of through-the-thickness stitching on the Mode I interlaminar fracture toughness of flax/epoxy composite laminates. Materials & Design. 2016 November; 109: 659-669.

5. Mouritz AP. Review of z-pinned laminates and sandwich composites. Composites Part A: Applied Science and Manufacturing. 2020 December; 139: 106-128.

6. Pascoe JA, Pimenta S, Pinho ST. Interlocking thin-ply reinforcement concept for improved fracture toughness and damage tolerance. Composites Science and Technology. 2019 September; 181: 107681.

7. Mouritz AP, Bannister MK, Falzon PJ, Leong KH. Review of applications for advanced three-dimensional fibre textile composites. Composites Part A: Applied Science and Manufacturing. 1999 December; 30(12): 1445-1461.

8. Goutianos S, Sørensen BF. Fracture resistance enhancement of layered structures by multiple cracks. Engineering Fracture Mechanics. 2016 January; 151: 92-108.

9. Tao R, Li X, Yudhanto A, Alfano M, Lubineau G. Laser-based interfacial patterning enables toughening of CFRP/epoxy joints through bridging of adhesive ligaments. Composites Part A: Applied Science and Manufacturing. 2020 December; 139: 1069094.

10. Trabal GG, Bak BLV, Chen B, Lindgaard E. An adaptive floating node based formulation for the analysis of multiple delaminations under quasi-static loading. Composites Part A: Applied Science and Manufacturing. 2022 May; 156: 106846.

11. Turon A, Camanho P, Costa J, Dávila C. A damage model for the simulation of delamination in advanced composites under variable-mode loading. Mechanics of Materials. 2006 November; 38(11): 1072-1089.

12. Lindgaard E, Bak BLV, Glud JA, Sjølund JH, Christensen ET. A user programmed cohesive zone finite element for ANSYS Mechanica. Engineering Fracture Mechanics. 2017 July; 180: 229-239.

13. Juntti M, Leif AE, Olsson R. Assessment of evaluation methods for the mixed-mode bending test. Journal of Composites, Technology and Research. 1999; 21(1): 37-48.

14. Bak BLV, Turon A, Lindgaard E, Lund E. A simulation method for high-cycle fatigue-driven delamination using a cohesive zone model. Numerical Methods in Engineering. 2016 August; 106(3): 163-191.

15. Mosbjerg SJ, Martos MJ, Bak BLV, Lindgaard E. Formulation of a mixed-mode multinlinear cohesive zone law in an interface finite element for modelling delamination with R-curve effects. Composite Structures. 2019 May; 216: 477-486.

16. Mosbjerg SJ, Martos MJ, Lindgaard E, Bak BLV. Inverse parameter identification of n-segmented multilinear cohesive laws using parametric finite element modeling. Composite Structures. 2019 October; 225: 111074.

17. Bak BLV, Lindgaard E, Lund E. A simulation method for high-cycle fatigue-driven delamination using a cohesive zone model. Internation al Journal for Numerical methods in Engineering. 2015 August; 106(3): 163-191.

18. Carreras L, Turon A, Bak BLV, Lindgaard E, Renart J, Martin de la Escalera F, et al. A simulation method for fatigue-driven delamination in layered structures involving non-negligible fracture process zones and arbitrarily shaped crack fronts. Composites Part A: Applied Science and Manufacturing. 2019 January; 122: 107-119.

19. Carreras L, Bak BLV, Turon A, Renart J, Lindgaard E. Point-wise evaluation of the growth driving direction for arbitrarily shaped delamination fronts using cohesive elements. European Journal of Mechanics. 2018 March; 72: 464-482.